AQUARIUS/SAC-D

Aquarius Salinity Validation Analysis

Aquarius Project Document: **AQ-014-PS-0016**
18 February 2013

Data Version 2.0

Aquarius Salinity Validation Analysis

PREPARED BY (CUSTODIAN):

__GARY LAGERLOEF____ _____
Name Date

APPROVED BY:

_____ _____
Name Date

_____ _____
Name Date

_____ _____
Name Date

DOCUMENT CHANGE LOG

Change Number	Change Date	Pages Affected	Changes/ Notes	General Comments
-	18 February 2013	All	Initial Release	

Aquarius Salinity Validation Analysis; Data Version 2.0

Lead Author: Gary Lagerloef (Earth & Space Research), Aquarius Principal Investigator
Contributing Authors: Hsun-Ying Kao (Earth & Space Research), Oleg Melnichenko (U University of Hawaii), Peter Hacker (U University of Hawaii), Erick Hackert (U University of Maryland, ESSIC), Yi Chao (Remote Sensing Solutions), Kyle Hilburn (Remote Sensing Systems), Thomas Meissner (Remote Sensing Systems), Simon Yueh (Jet Propulsion Lab), Liang Hong (Goddard Space Flight Center), Tony Lee (Jet Propulsion Lab)

1. Introduction

The purpose of this report is to document the Aquarius sea surface salinity (SSS) measurement error statistics and some residual errors in the V2.0 data release. We also document the effect that changes in the science data processing since V1.3 have on the error statistics by comparing V1.3 with V2.0 results. In this analysis, we used an interim test data set named V1.3.9, which is the same processing code that is used for V2.0. Accordingly, all the analyses and figures here refer to V2.0 when in fact the calculations were done with V1.3.9 test data files.

Although considerable improvements have been achieved since V1.3, there are a number of issues affecting the scientific interpretation of the V2.0 data. These are detailed in the report and summarized in the last section (**Summary, Conclusions and Cautions).**

Readers of this document are assumed to be familiar with the Aquarius/SACD mission and sensor design, sampling pattern, salinity remote sensing principles, and pre-launch error analysis as described by [1] and [2]. It is particularly relevant to the error analyses to understand that the measurement sensitivity is proportional to sea surface temperature (SST), so that the salinity data are more prone to errors in the high latitudes than in the tropics. It should also be noted that a post-launch 0.5 degree pointing bias has been determined and corrected between V1.3 and V2.0 algorithms, which affects both the measurement incidence angle and geo-locations of the data between versions. This information is documented in [3].

The sensor calibration is done with a forward model to estimate the antenna temperature at the satellite, then differencing that estimate from the measured antenna temperature on a global average [4]. The forward model includes the surface emission, geophysical corrections, antenna pattern correction, etc. An important achievement in the V2.0 data is separating the sensor calibration variations from time-varying errors in the geophysical corrections, as described in [4]. This has removed the quasi-monthly, non-monotonic, variations previously seen in the V1.3 data.

The surface emission for the forward model is derived from ancillary SST and SSS. The SST data are derived from the daily high-resolution blended SST produced by NOAA National Center for Environmental Prediction (NCEP) as described in [5]. The SSS are derived from the US Navy HYbrid Coordinate Ocean Model (HYCOM) daily averaged data-assimilative analysis ([6] and Appendix A). The operational data are produced by the U.S. Naval Oceanographic Office (NAVO), but the digital output are distributed by Florida State University. Therefore HYCOM salinity is used as a global surface calibration target for the sensor, whereas validation of the salinity output is done with surface *in situ* buoy data. The basic principle, therefore, is to *calibrate* with HYCOM globally, and *validate* with buoy data locally, although HYCOM salinity is also considered with buoy data in some of the global statistical error analyses.

The Aquarius project produces three data sets: Level 1a (raw data), Level 2 (science data in swath coordinates and matching ancillary data), and Level 3 (gridded 1-degree daily, weekly and monthly salinity and windspeed maps). This validation analysis will start with Level 2 data evaluation followed by Level 3 on monthly and seasonal (3-month) averages. Salinity measurements are on the practical salinity scale (PSS-78), technically a dimensionless number, but in some figures labeled as practical salinity units (psu).

2. Matchup maps and differences

We start with global maps comparing the Aquarius Level 2 samples with surface *in situ* Argo buoy data (Figure 1). The Argo data are generally sampled at a shallowest depth of 3-5 meters from the surface. Under most conditions (e.g., moderate to high winds) the surface ocean mixed layer extends much deeper, and the buoy provides an accurate measure of the 1-2 cm surface layer that emits the microwave signal seen by the satellite. However, under persistently rainy conditions, there are often gradients between the surface and the buoy measurement depth. The Aquarius Level 2 (swath) data are taken at the closest point to a buoy. The time window is ± 4.5 days to gather all buoy data within the 7-day orbit repeat cycle (analysis shows that ± 3.5 day window has negligible effect on standard deviations). The search

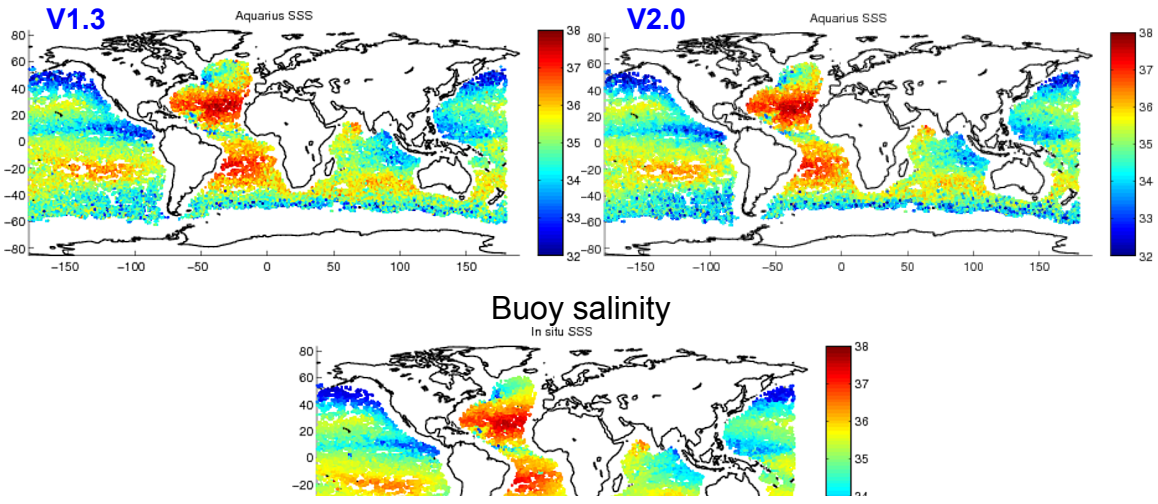

radius is 75 km between the buoy location and the bore sight position of the Aquarius footprint. The Aquarius data are averaged over 11 samples (~100 km) centered on the match-up point. Argo buoys surface once every 10 days and remain at the surface for a few hours. The time of day is random.

Figure 1 shows the Aquarius retrieved salinity at the buoy matchup points for the first 16 months of observations. Aquarius V1.3 and V2.0 data and the buoy data at the same matchup points are shown. The correspondence is visibly quite clear with Aquarius Level 2 data resolving the salient large scale ocean features, albeit somewhat more noisy, especially in the extreme southern latitudes.

Figure 2 shows the Aquarius-Argo differences with these same match-ups for V1.3 and V2.0. One conspicuous improvement evident in V2.0 is in reducing the persistent positive bias that V1.3 has in the Southern Ocean. Other systematic improvements less visible here will be demonstrated by related analyses below.

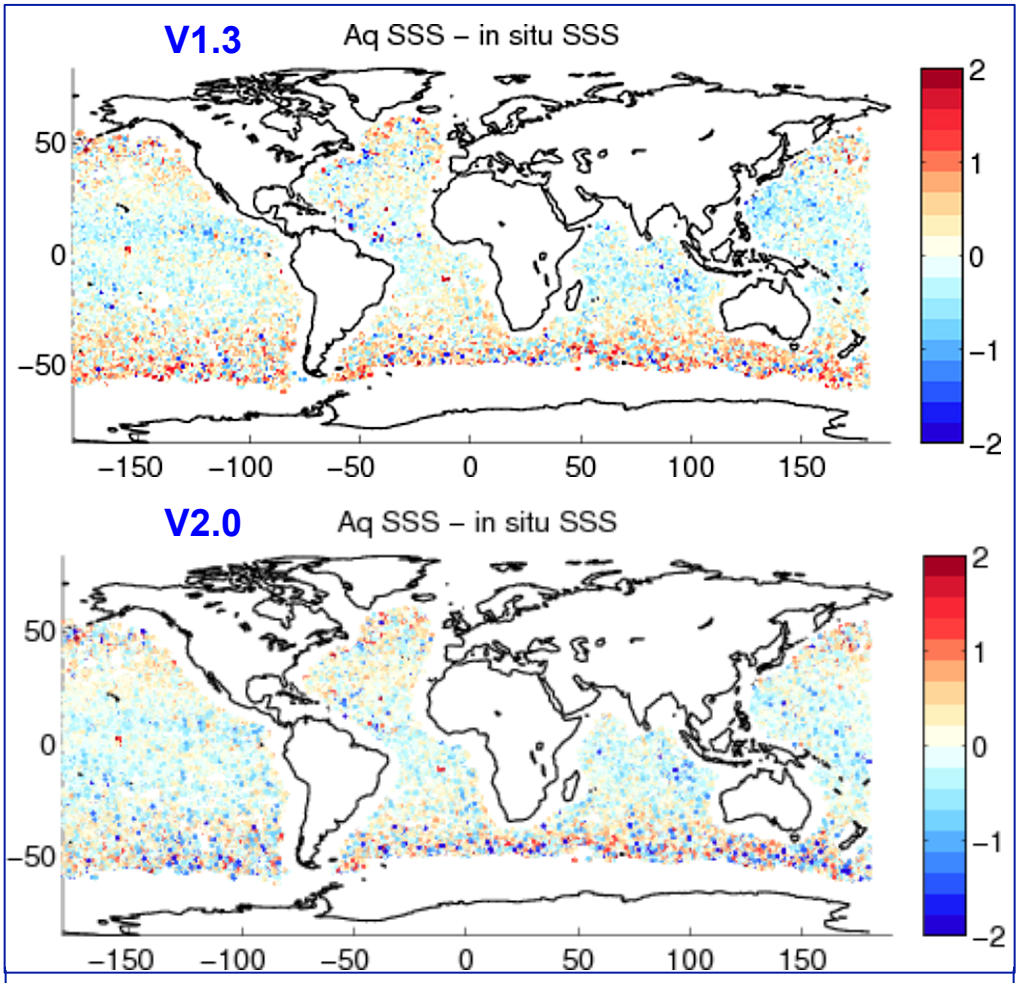

Figure 2. . Global maps of SSS differences as defined by the Aquarius V1.3 (top) and V2.0 (bottom) data minus the co-located buoy data.

3. 3-beam histograms (V1.3 & V2.0)

Histograms of the matchup salinity differences for each of the three beams are in Figure 3. In these statistics, we excluded colocations that add considerable noise and skewness to the data (SST < 5C, Windspeed > 15 m/s, and gain-weighted land and ice fractions >0.0005). There is a measureable improvement of the bias (median) in Beams 1 and 2, and reductions in the standard deviations in all three beams. The root mean square difference (RMSD), which is the root sum square (RSS) of the bias and standard deviation, is reduced from ~0.55 in V1.3 to ~0.50 in V2.0. These are the ensemble statistics for the 16-month record of global ice-free ocean data.

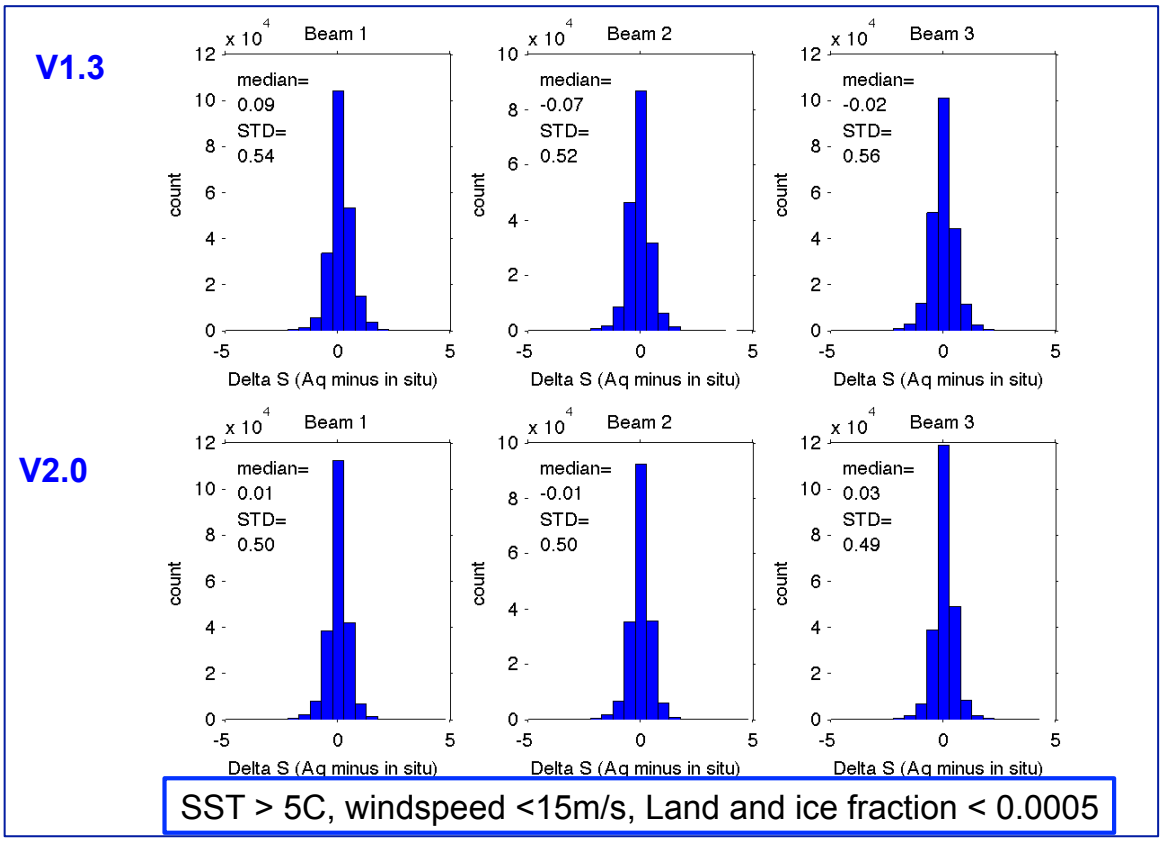

Figure 3. Histograms for Aquarius - buoy differences, V1.3 (top), V2.0 (bottom).

Scatter plots between the Aquarius V2.0 and buoys are shown for each beam in Figure 4. The color contours represent the density of points, and fit is quite linear

over the open ocean salinity dynamic range. Some outliers (faint yellow color) are evident with in situ salinity at about 34, and Aquarius data are biased low. These points are generally in the high latitudes.

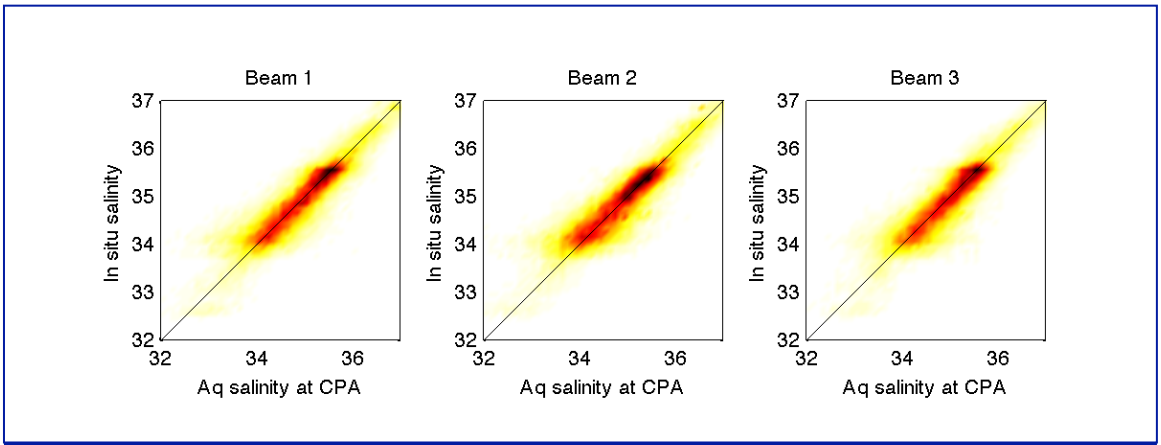

Figure 4. Scatter plots of V2.0 Aquarius (abscissa) and co-located buoy data (ordinate) for each beam.

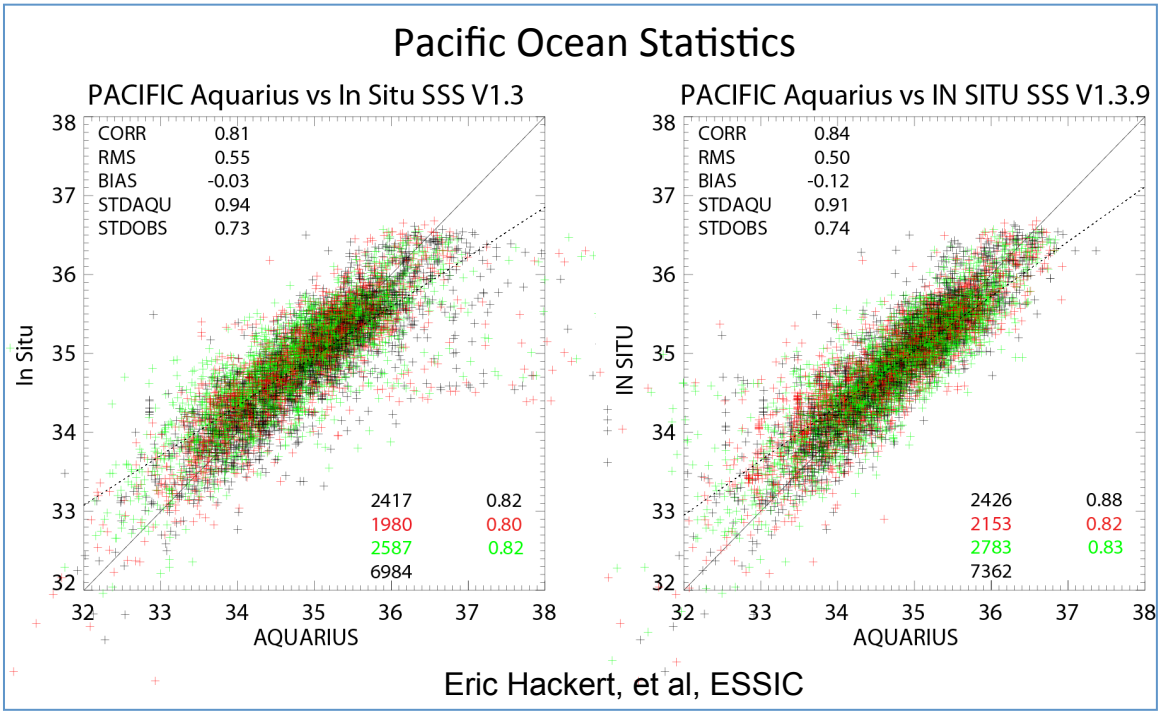

Figure 5. Alternate co-located in situ data statistics in the tropical Pacific contributed by Eric Hackert, U. Maryland, ESSIC. (Left) V1.3, (Right) V1.3.9 proxy of V2.0.

Corroborating matchup analyses are in Figure 5, in this case using a variety of in situ sources, including Argo, TAO moorings, etc, from the GTSPP between 30N and 30S latitude, and matchups for each beam (colors) within 1 degree (lat/lon) and 1 day. The Pacific statistics are similar to the global results given above with RMSD ~0.55 and 0.50 for V1.3 and V2.0 respectively. For the tropical Indian Ocean, the RMSD

drops from 0.52 to 0.49 for V1.3 and V2.0 but the RMSD for the tropical Atlantic (not shown) were somewhat lower, ~0.45, for both data sets.

The HYCOM data are used as a salinity reference for evaluation and global calibration [4]. The HYCOM surface salinity is interpolated to the time and location of every 1.44 second sample interval in Aquarius Level 2 data files. Here, in Figure 6, these reference salinity data are evaluated against the Argo measurements with the same matchup processing as Aquarius Level 2 data. The results are shown separately for the ascending (northward) and descending (southward) halves of the orbit. The first feature to emphasize is that there is no systematic difference between the ascending to the descending passes for the buoy and HYCOM salinity difference. This continuity is noteworthy because of the ascending – descending differences found in the Aquarius measurements addressed in detail in a later section. Secondly, it is clear that there are regional long-term systematic biased between HYCOM output and the buoy data. HYCOM is biased positive relative to the Argo buoys in the Circumpolar current, tropics and North Pacific. Over much of the mid latitudes the bias is slightly negative. These differences exist even though most of the in situ data we are using here are assimilated by HYCOM and therefore not fully independent data.

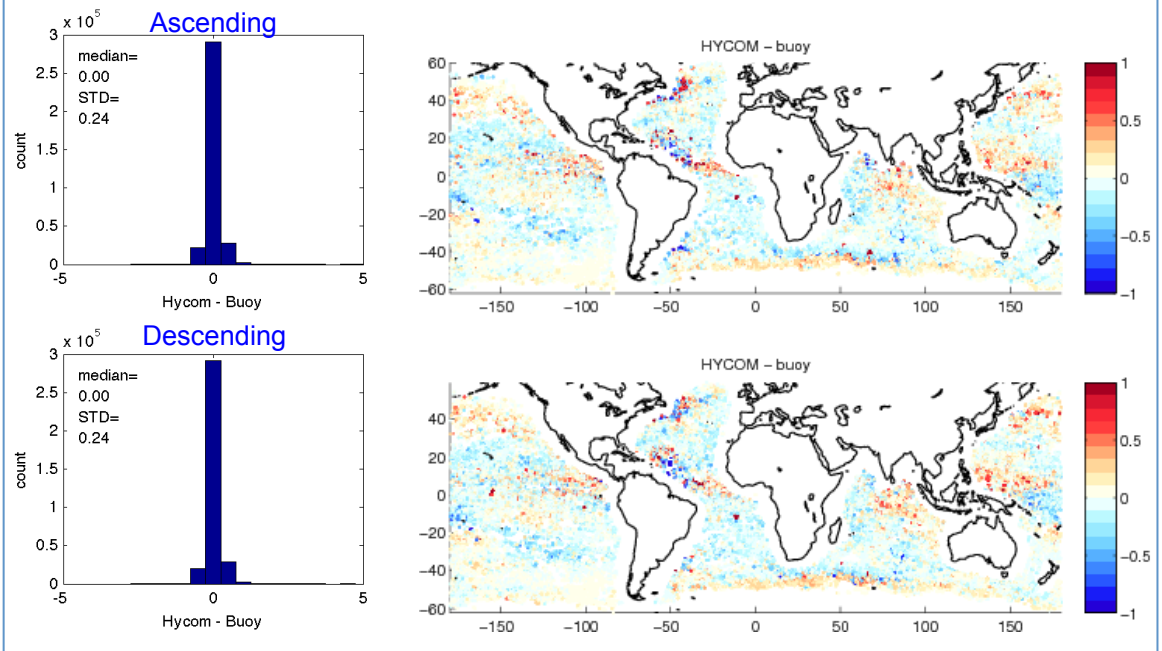

Figure 6. Co-located salinity differences between HYCOM and buoys for ascending (top) and descending (bottom) passes.

The histograms and statistics in Figure 6 demonstrate that for the global average, the HYCOM-buoy differences have no bias, either for ascending or descending passes. This is a relevant point for validating our overall calibration approach because we use the HYCOM salinity as a surface reference for modeling the on-orbit antenna temperatures for calibrating the sensors [4]. We compute these calibrations on a global scale with running averages that use all orbits in a 7-day repeat cycle. In contrast, the HYCOM-buoy regional differences demonstrate that regional or zonal calibrations will be problematic, and we have used only global analyses for calibration.

4. Triple point analysis

Figure 7 gives the V2.0 matchup statistics for Aquarius-buoy, HYCOM-buoy, and Aquarius-HYCOM (at the buoy locations), for each of the three beams. These show HYCOM-buoy RMSD ~0.25 overall. (This is a decrease of previous estimates ~0.32 because of a geo-location error of the interpolated HYCOM data in V1.3 that has since been corrected in V2.0. This corrupts the colocation statistics using HYCOM, and thus V1.3 triple-point analyses are not used). The RMSD for Aquarius-buoy and Aquarius-HYCOM are essentially the same. The co-located statistics allow us to estimate the root mean square error (RMSE) of each of the three measurements (*See Appendix B*). These results are given in Table 1, where the Aquarius RMSE are ~0.46 and the HYCOM and buoy RMSE are ~0.17 to 0.18. Recall that these Aquarius matchup statistics are for individual measurements, with no averaging. The idealized monthly average RMSE is possibly as low as ~0.17, assuming a minimum of 8 samples per month and uncorrelated errors, as seen in the lower panel of Table 1. Directly computed monthly statistics are not this small, as will be discussed in a later section.

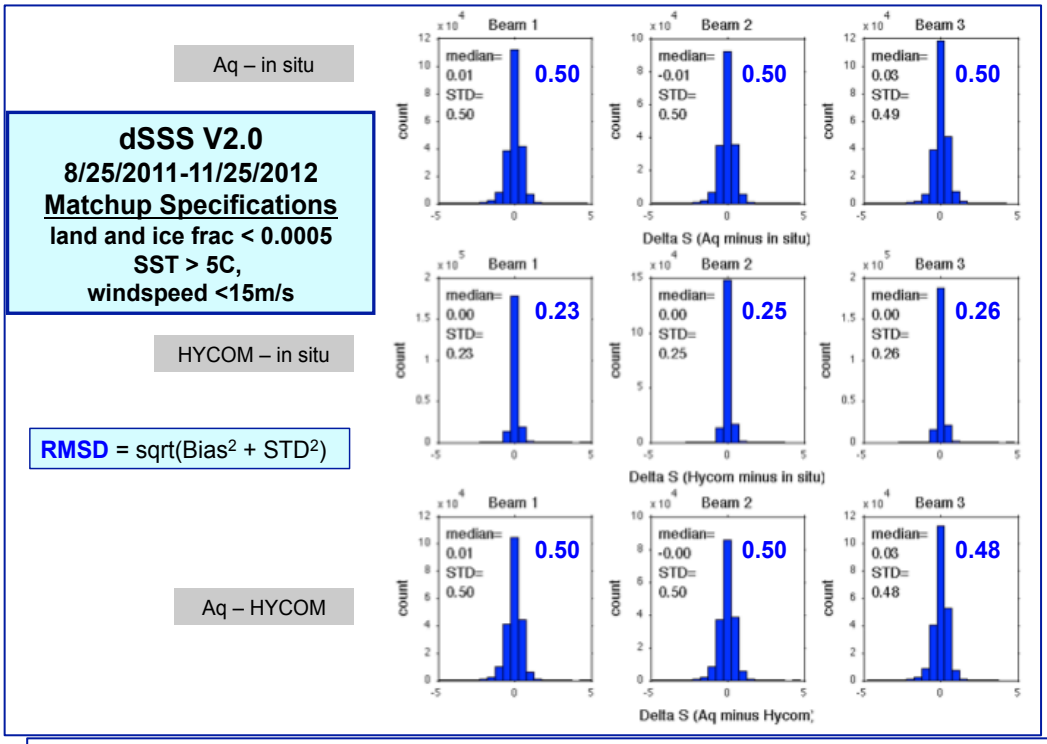

Figure 7. Co-located difference histograms for each beam and Aquarius V2.0 data. (top) Aquarius-*in situ*, (middle) HYCOM - *in situ*, (bottom) Aquarius - HYCOM.

	Beam 1	Beam 2	Beam 3
Aquarius RMSE	0.47	0.47	0.45
Hycom RMSE	0.16	0.18	0.17
Insitu RMSE	0.16	0.18	0.20
Theoretical monthly RMSE if all errors are uncorellated			
Monthly RMSE (8 samples worst case) psu	0.17	0.17	0.16

Table 1. Estimated Root Mean Square Error (RMSE) for each data type based on the triple point analysis of co-located point measurements.

5. Buoy matchup time series (V1.3 & V2.0)

A key milestone in V2.0 data processing relates to the sensor calibration. This has now effectively corrected the non-monotonic, quasi-monthly variations, which we often refer to as 'wiggles'. Figure 8 shows how these calibration errors affect the global average salinity bias over time, and how the V2.0 has effectively removed them [4]. These time series curves are global daily median values of Aquarius-buoy matchup data. During the first half of the record, V1.3 curves show the quasi-monthly calibration variations, which translated into global average salinity errors ± ~0.2 psu. V2.0 data over the same time period show that these have been effectively removed. This was done with radiometer calibration adjustments described in [4], not as adjustments to retrieved salinity.

Although the quasi-monthly wiggles are gone, and the V2.0 calibrations are considerably more stable, the V2.0 time series does show smaller calibration drifts with near-annual time scale. These spurious signals persist in the data primarily from errors in the geophysical corrections, and will be discussed in more detail below starting with Section 6.

During the second half of the record, V1.3 data show numerous spikes, which coincide with satellite maneuvers or safe-hold events that interrupted the normal spacecraft nadir pointing. V2.0 data has additional parameters and flags to ensure these episodes are adequately identified in the Level 2 data, and can be rejected as needed in subsequent analyses such as these. The spacecraft attitude control parameters and flags are described in the Aquarius data users guide.

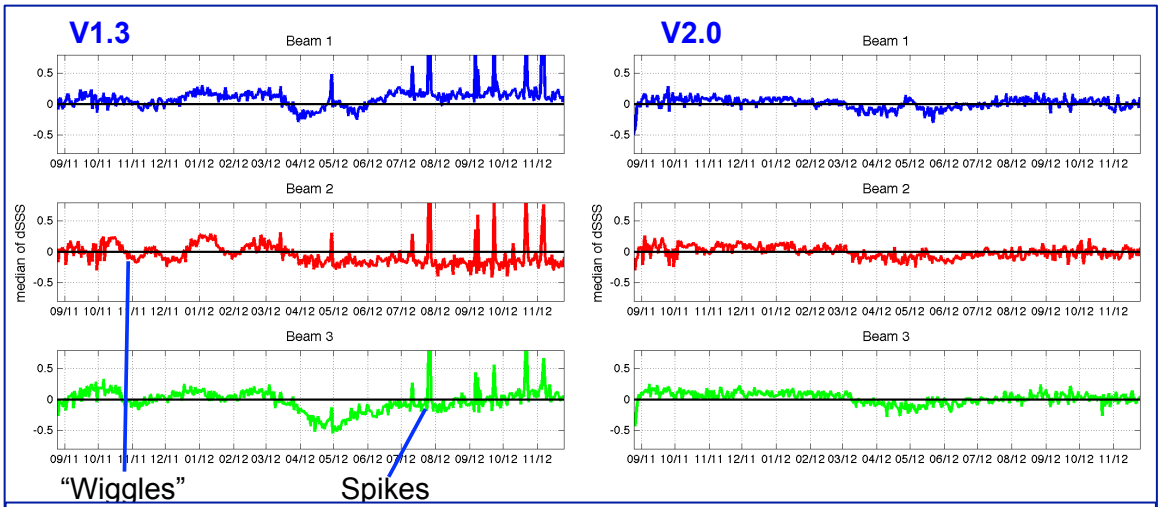

Figure 8. Daily global average Aquarius-buoy difference time series, V1.3 (left) and V2.0 (right).

6. Monthly and seasonal buoy matchup maps

Next, we examine buoy difference statistics of monthly 1x1 degree Level 3 salinity data maps. The Level 3 maps are generated from Level 2 salinity data without any added adjustment for climatology, reference model output or *in situ* data. The smoothing interpolation applies a bi-linear fit within a specified search radius. Most of the results shown here are computed using a ~150 km radius, and exclude data where the land or ice fractions exceed 0.0005 (ESR data), which are restricted to open ocean conditions. We also show results from the Aquarius standard monthly Level 3 data which are presently gridded with a 2 degree lat-lon radius and excludes land-fraction >0.02 and ice-fraction >0.005, which therefore are less restricted to open ocean. The buoy matchups are compiled for each 1-degree grid with an average of the buoys within the 150 km radius and with buoy SST>5C.

Results for V1.3 data are shown in Figure 9. The tabulated monthly standard deviations range from 0.42 to 0.54 for the 10-months shown. A seasonal change in the pattern of buoy differences is evident, with more positive bias, mainly in the Southern Hemisphere, from September 2011 – February 2012, then changing to a negative bias the remaining months. The bias is generally negative throughout the tropics during most the months shown.

ESR gridding
land and ice frac < 0.0005
Buoy SST>5C, radius=150km

	median	STD
SEP/11	0.08	0.46
OCT/11	0.08	0.44
NOV/11	-0.02	0.54
DEC/11	0.06	0.54
JAN/12	0.10	0.50
FEB/12	0.10	0.50
MAR/12	-0.03	0.42
APR/12	-0.23	0.46
MAY/12	-0.21	0.42
JUN/12	-0.08	0.45

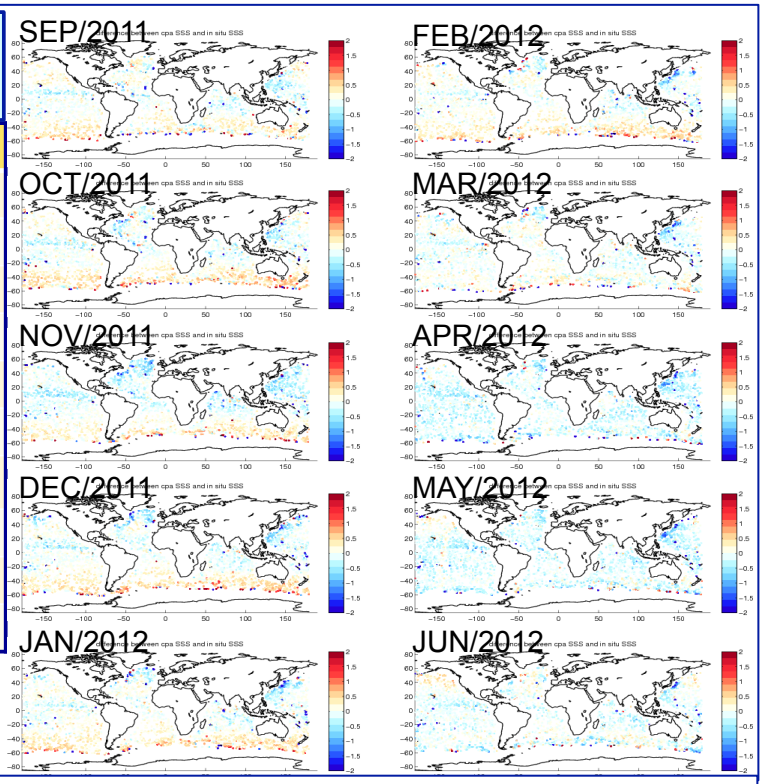

Figure 9. V1.3 Aquarius monthly difference maps and statistics.

The contrasting V2.0 results appear in Figure 10. The table shows that the monthly standard deviations are considerably (~30%) less than V1.3. Note also that the color scale is reduced by 2:1 for the maps. The same basic seasonal pattern is still prevalent between the austral fall and spring. This is a spurious seasonal signal in the Aquarius V2.0 data. It appears amplified in the higher latitudes, especially in the Southern Hemisphere. The table shows consistent positive global mean bias for the months September through February, and negative bias March through August.

Monthly global RMSE is less than V1.3, but geographically correlated errors remain (lower range color scale)

	median	STD
SEP/11	0.07	0.30
OCT/11	0.07	0.33
NOV/11	0.07	0.35
DEC/11	0.05	0.35
JAN/12	0.06	0.35
FEB/12	0.02	0.37
MAR/12	-0.10	0.33
APR/12	-0.13	0.31
MAY/12	-0.11	0.31
JUN/12	-0.07	0.33
JUL/12	-0.03	0.34
AUG/12	-0.03	0.36
SEP/12	-0.01	0.29

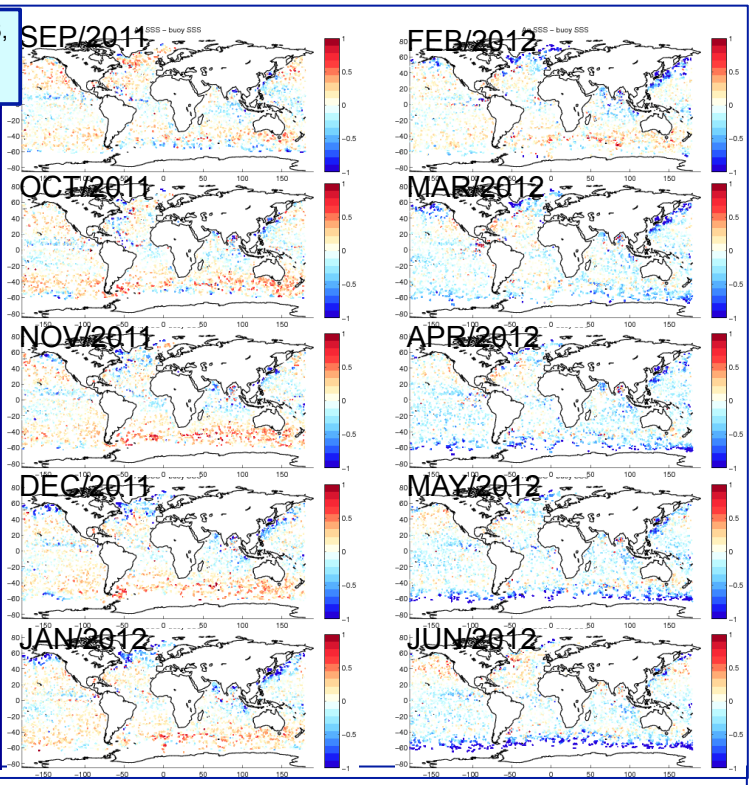

Figure 10. Same as Figure 9 for V2.0 Aquarius data. Note that the errors are much reduced from V1.3. The color scale on the difference maps is half that in Figure 9.

Figure 11 shows the corresponding results for the standard Aquarius Level 3 data produced by the Aquarius Data Processing System (ADPS) using the same basic gridding algorithm with a few slightly relaxed parameters for excluding data from the gridding. The same seasonal error pattern is evident. The standard deviations are somewhat greater because of the different land and ice exclusions applied.

ADPS gridding
land_frac <0.02; ice_frac <0.005
Higher AQ-buoy STD

	median	STD
SEP/11	0.07	0.37
OCT/11	0.07	0.37
NOV/11	0.06	0.37
DEC/11	0.05	0.38
JAN/12	0.05	0.40
FEB/12	0.02	0.41
MAR/12	-0.10	0.37
APR/12	-0.14	0.37
MAY/12	-0.11	0.36
JUN/12	-0.07	0.37
JUL/12	-0.03	0.37
AUG/12	-0.01	0.36
SEP/12	0.01	0.35

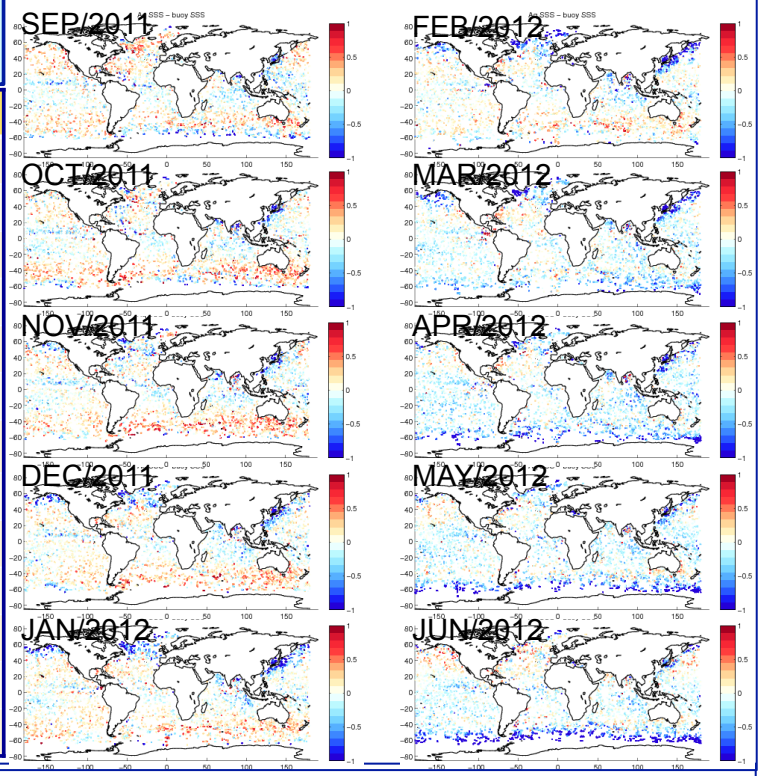

Figure 11. Same as Figure 10, for V2.0 Aquarius Data Processing System (ADPS) L3 monthly gridded data.

7. Contrasting Ascending and Descending passes

We now examine the differences between the ascending (northward, 6pm) and descending (southward, 6am). These show several residual modeling issues in the V2.0 data. In principle, the ascending and descending maps are expected to be nearly identical (e.g. Figure 6). Here we use a 10-month block of data from September 2011 through June 2012. The ascending-descending map for V1.3 (Figure 12) shows several areas of concern with biases much in excess of 0.2. In the Northern Hemisphere, a large blue patch in the eastern Atlantic, and red zones in the western Atlantic and Asian Pacific are believed to be related to low-level radio frequency interference (RFI) from adjacent land areas that leaks through the antenna side lobes and is not detected by the standard RFI filter algorithm. This causes a positive brightness temperature bias and thus a negative salinity bias. The RFI asymmetry between ascending and descending is the result of the opposite viewing angle (toward or away from the land emitting sources) between the two sides of the orbit. The antenna faces eastward on ascending passes and westward

on descending passes. Significant progress in modeling this effect is being made and is documented in [4].

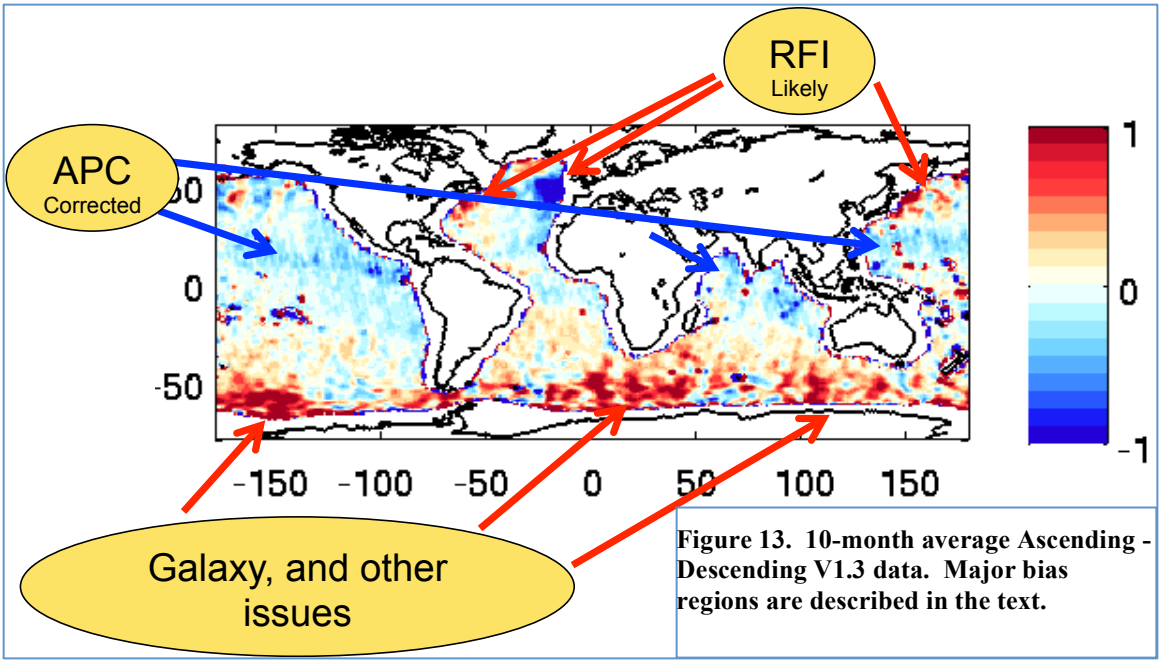

Figure 13. 10-month average Ascending - Descending V1.3 data. Major bias regions are described in the text.

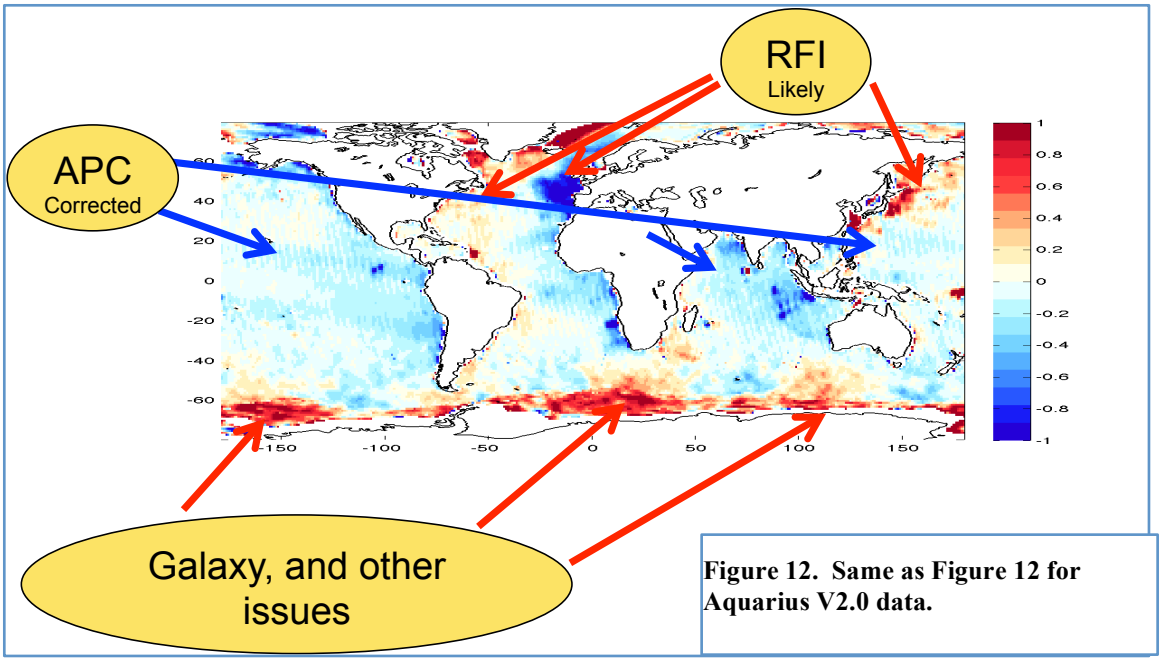

Figure 12. Same as Figure 12 for Aquarius V2.0 data.

In the tropics, the east-west blue colored band is aligned with the magnetic equator and related to antenna pattern correction (APC) cross-polarization coupling that affects ionosphere corrections. These have been mostly corrected in the V2.0. The Southern Hemisphere biases are likely to be related to the galaxy reflection term that is not correctly adjusted for wind. As we will see below, this has a strong annual cycle and largely accounts for the annual biases discussed earlier.

For V2.0 (Figure 13), shows that these patterns are essentially unchanged, especially the northern RFI patterns and the southern ocean.

Figures 14 and 15 show the buoy difference statistics in discrete latitude bands for ascending, descending and both (entire orbit), and for the V1.3 and V2.0 data respectively. For V1.3, the bias is accentuated in the Southern Hemisphere (blue curve of the median bias). Standard deviations are lowest in the tropics and highest in the high latitudes. The ascending biases are most negative in the tropics. The V2.0 standard deviations are somewhat reduced relative to V1.3, and the north-south asymmetry of the median bias is much less conspicuous. V2.0 ascending biases are still negative in the tropics.

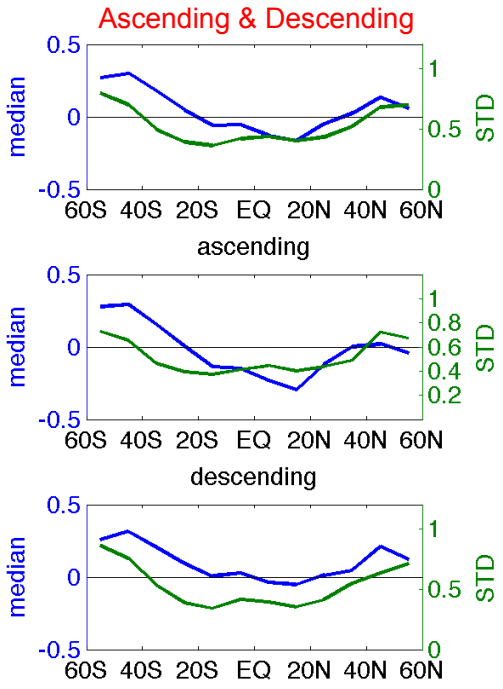

STD	both	ascend	descen
50-60N	0.70	0.67	0.71
40-50N	0.68	0.72	0.63
30-40N	0.52	0.49	0.55
20-30N	0.43	0.44	0.41
10-20N	0.40	0.40	0.35
0-10N	0.44	0.45	0.39
10S-0	0.42	0.41	0.41
10-20S	0.36	0.37	0.34
20-30S	0.39	0.39	0.39
30-40S	0.49	0.46	0.53
40-50S	0.70	0.65	0.76
50-60S	0.79	0.73	0.86

Figure 14. Aquarius V1.3 gridded data co-located buoy differences by latitude bands, all data from Sep 2011 through Dec 2012.

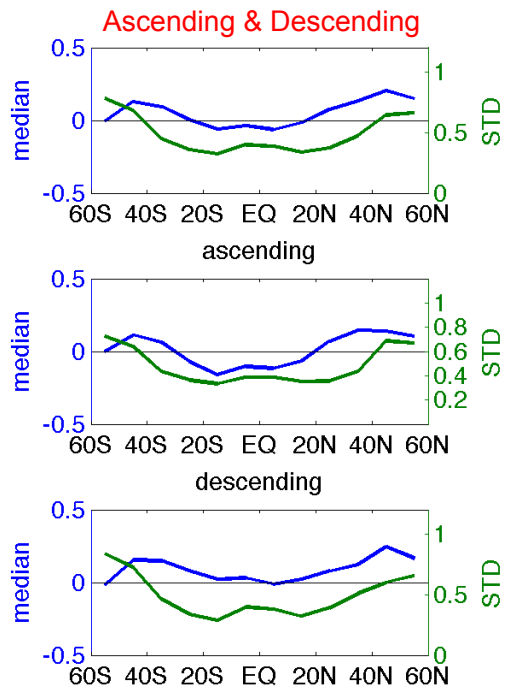

STD	both	ascend	descen
50-60N	0.66	0.67	0.65
40-50N	0.64	0.69	0.60
30-40N	0.47	0.43	0.51
20-30N	0.37	0.35	0.39
10-20N	0.34	0.35	0.32
0-10N	0.39	0.39	0.38
10S-0	0.40	0.39	0.40
10-20S	0.32	0.34	0.29
20-30S	0.36	0.36	0.34
30-40S	0.45	0.43	0.46
40-50S	0.68	0.64	0.72
50-60S	0.78	0.72	0.84

Figure 15. Same as Figure 14 for Aquarius V2.0 data.

8. Ascending – descending bias variations over time

Figures 16 and 17 contrast the variability of V1.3 and V2.0 global average deviations from buoy measurements in ascending-only matchups, descending-only, and the ascending-descending differences. One sees that the removal of the quasi-monthly calibration errors and the maneuver spikes in V2.0 provides a much cleaner record. It is also evident that longer timescale offsets are present in both V1.3 and V2.0, and that the ascending trends differ from descending in both versions, though more clearly resolved in V2.0. The ascending signatures for each of the three beams are similar one-another, and the inter-beam similarity is even more apparent in the descending data. The descending pass has a similar annual variation in each of the three beams. When the ascending and descending are combined, the longer term variations mostly offset one another (Figure 8). However the annual variability is accentuated in the ascending-descending signatures in Figures 16-17, which provide a robust indicator of residual data errors.

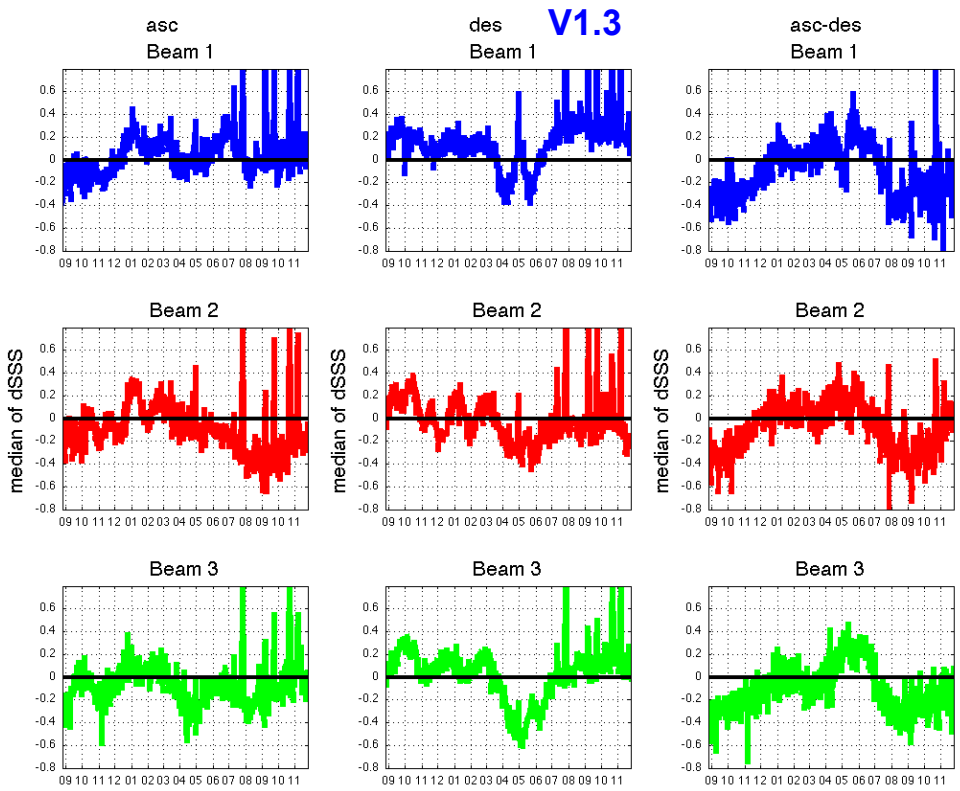

Figure 16. Daily average ascending and descending Aquarius-buoy difference time series, V1.3 data.

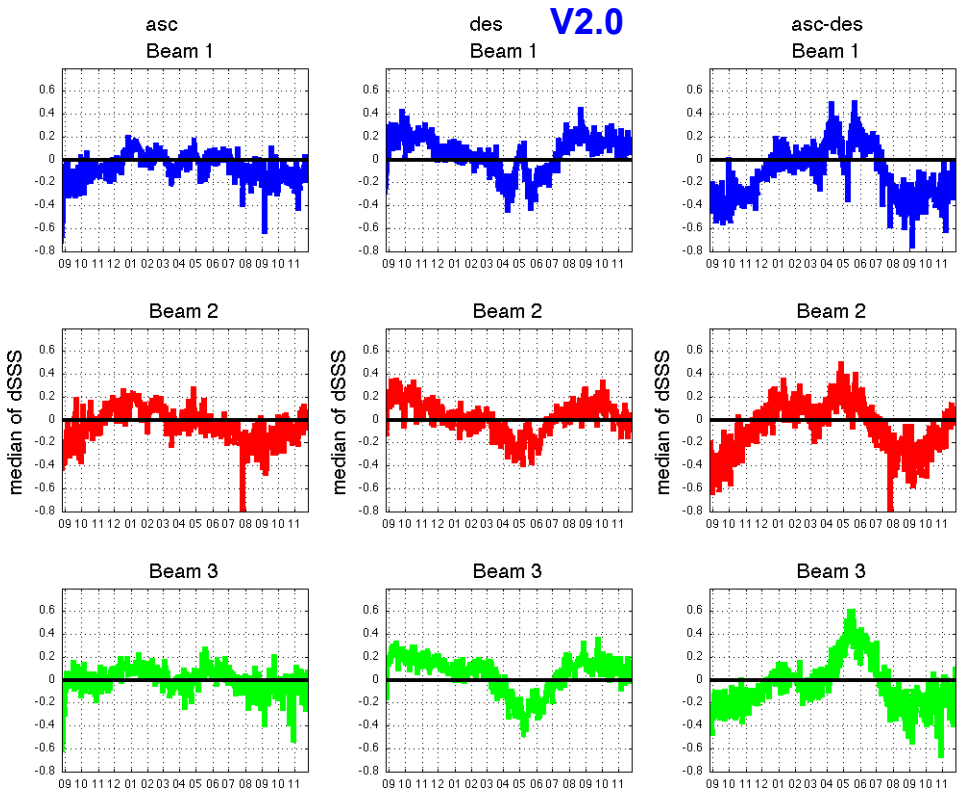

Figure 17. Same as Figure 16 for Aquarius V2.0 data.

The next several figures, illustrating ascending-descending maps, were provided by O. Melnichenko and P. Hacker from U. Hawaii. Figure 18 shows V1.3 and V2.0 ascending-descending maps for the month of September 2011, again illustrating that not much has changed between these two data versions.

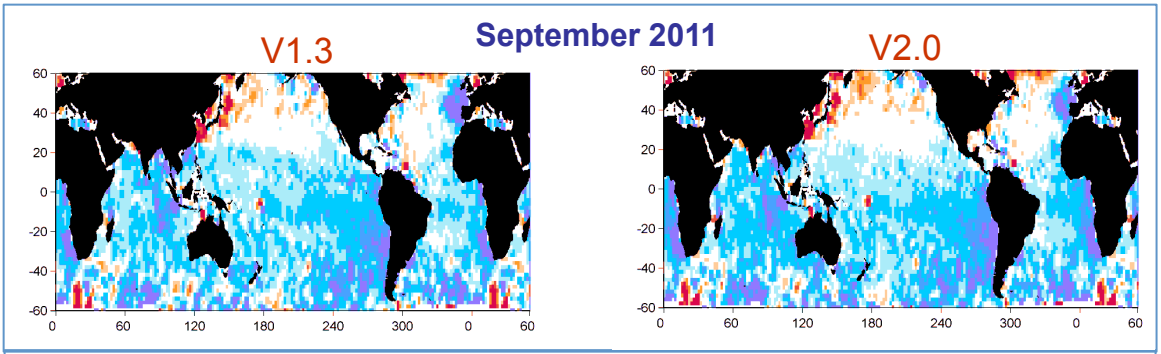

Figure 18. Ascending minus descending maps for September 2011 showing negligible difference between versions.

In figures 19 and 20 V2.0 data are utilized to illustrate the magnitude and geographic pattern of the seasonal ascending-descending changes on a monthly basis, which are accentuated in the Southern Hemisphere. The Northern Hemisphere RFI zones described earlier are persistent year-round.

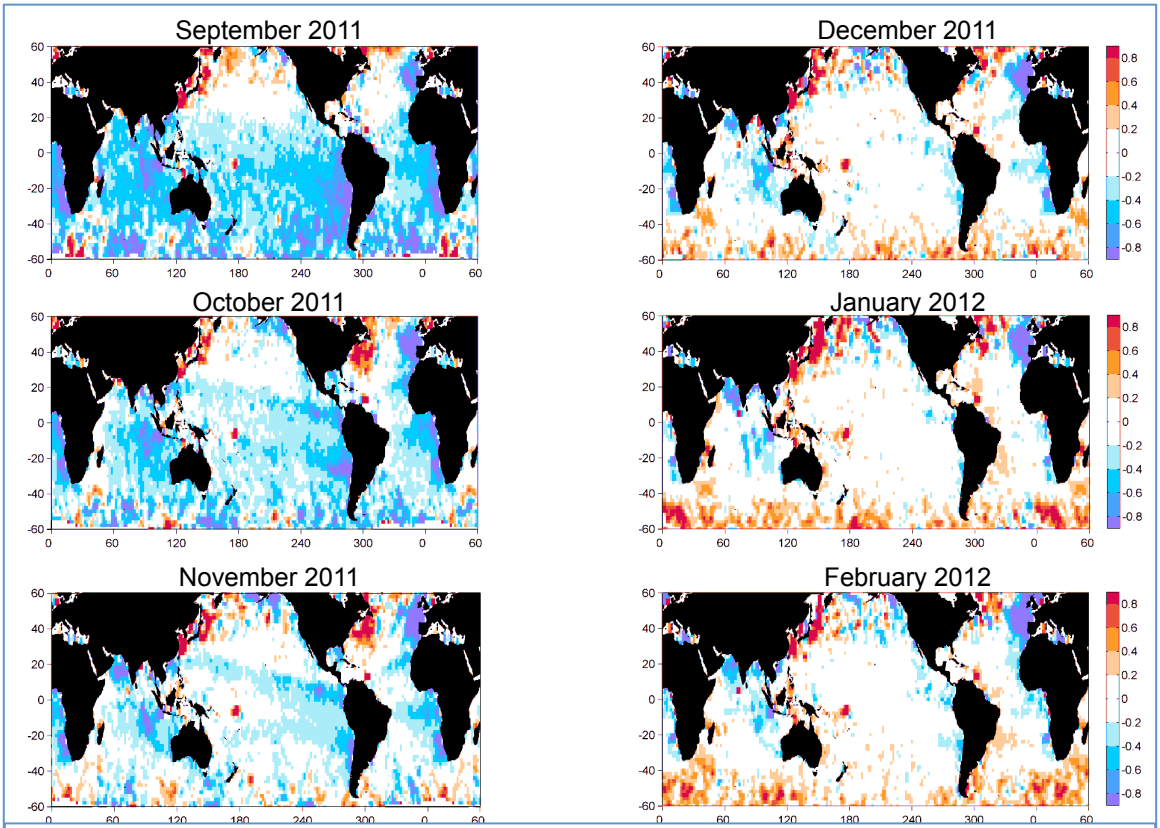

Figure 19. V2.0 ascending minus descending maps for September 2011 through February 2012 showing the seasonal progression. Results are similar in V1.3 (not shown).

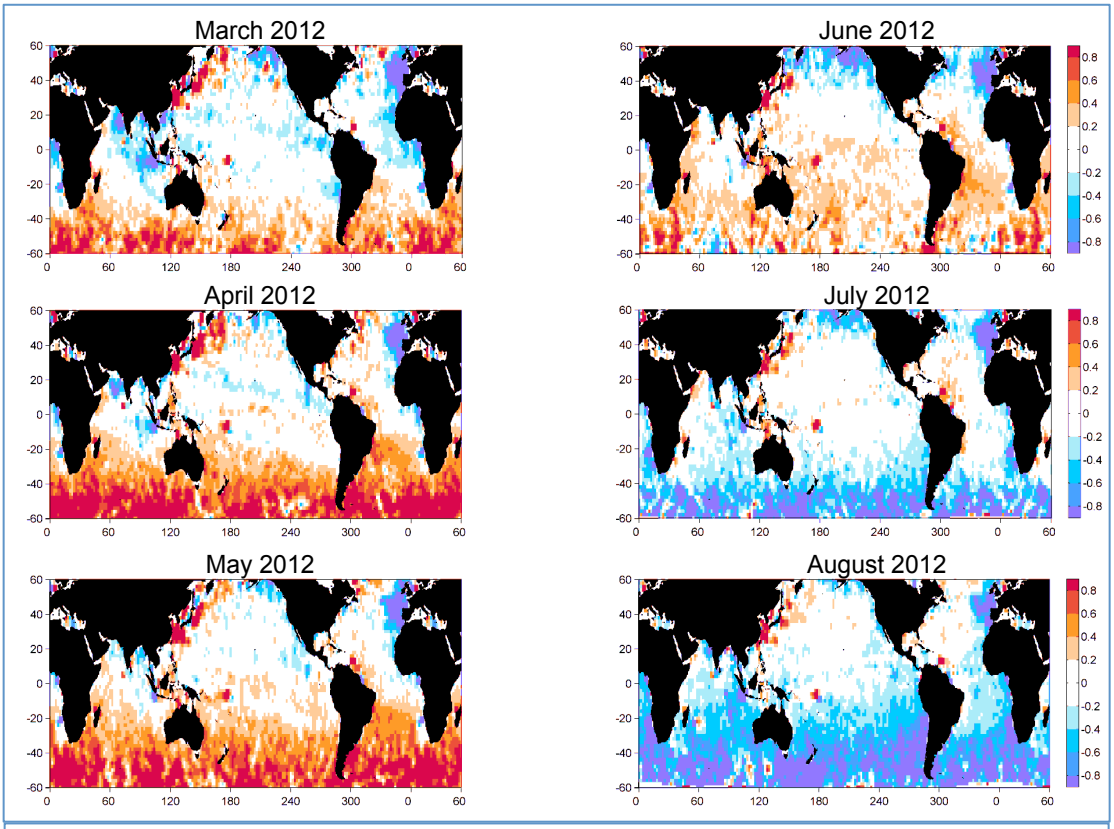

Figure 19. Same as Figure 19 except for March-August 2012.

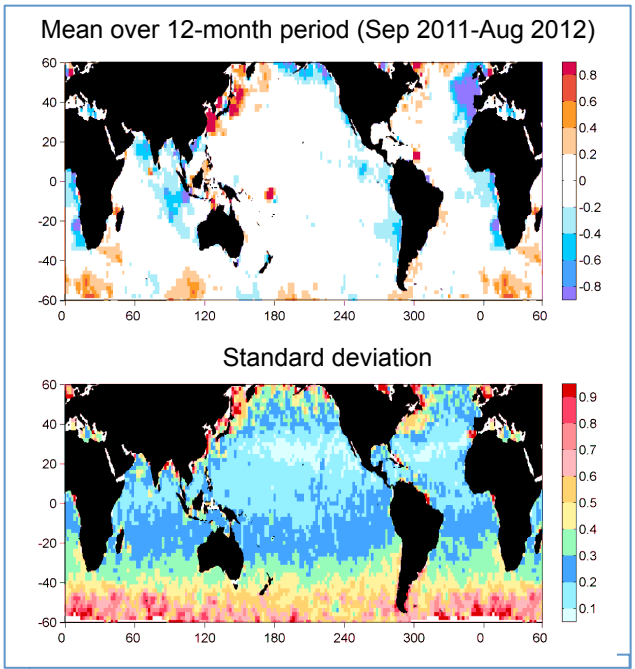

Figure 20. Mean and standard deviation of 12 monthly mean ascending - descending maps.

Figure 21 shows a 12-month average and standard deviation. The annual mean is mostly blank, and ideally how the individual months should appear. The near-zero annual average over most of the globe is another strong indicator of a seasonally related phenomenon. The standard deviation shows a clear zonal pattern, maximum in the highest latitudes.

An additional illustration is based on the Combined Active Passive (CAP) algorithm [7] and [8], which shows similar monthly biases (Figure 22). CAP uses both vertically and horizontally polarized surface brightness

temperatures (prior to roughness correction), including all the geophysical corrections, APC and sensor calibrations. (The standard L2 algorithm uses only vertically polarized brightness tempreatures for retrieval.) The distinct zonal banding during September-October across the tropical Pacific and Atlantic is visible in both analysis, but more so in CAP. This may indicate that the APC cross coupling needs further analysis. This is especially important to studies of the high-rainfall inter-tropical convergence zone (ITCZ), which aligns with much of this zonal error band in the Pacific.

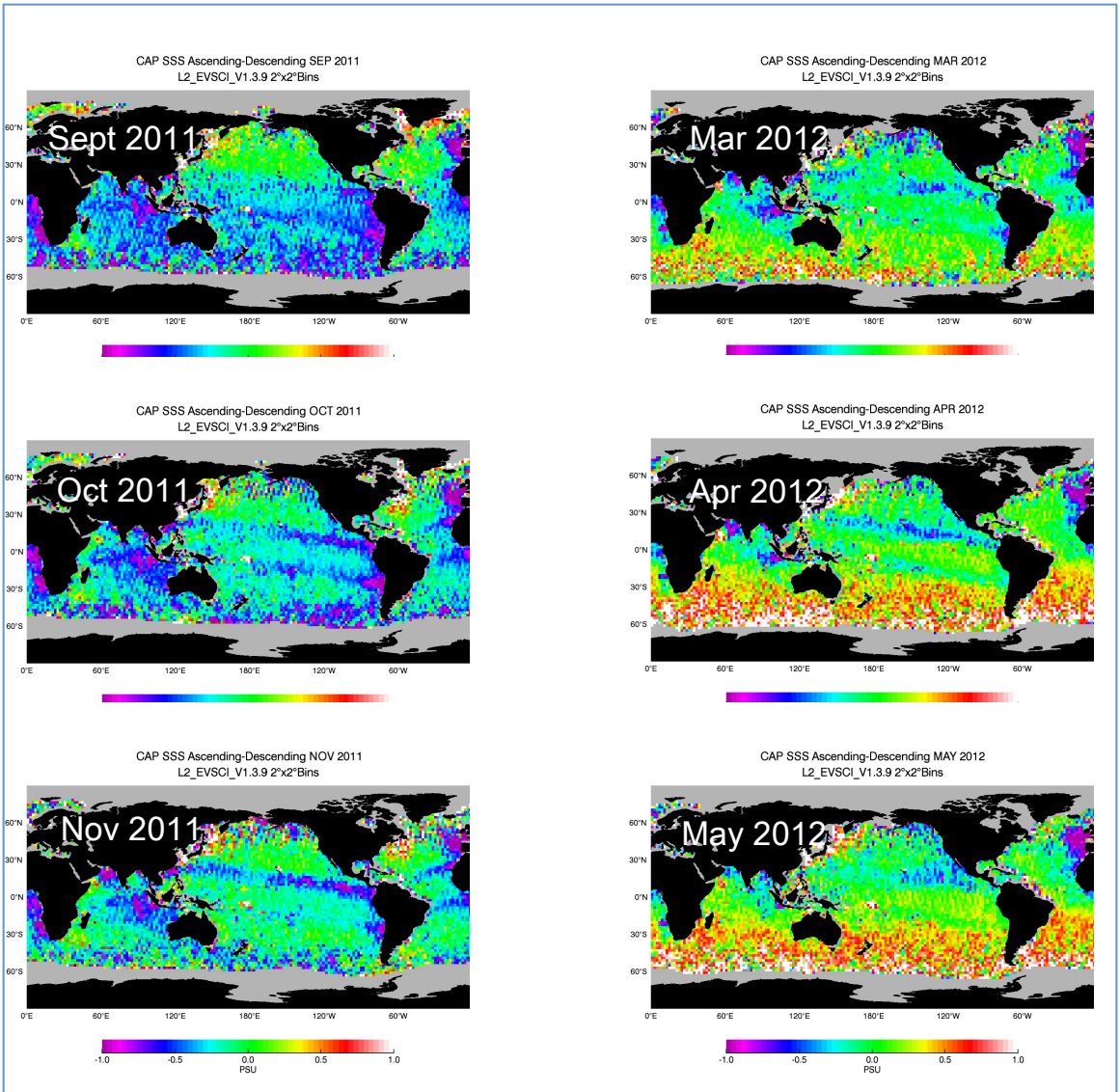

Figure 21. Opposite season ascending - descending maps from the CAP algorithm, showing similar patterns as Figures 19 and 20, and more conspicuous zonal bands in the fall.

These ascending-descending differences are the manifestation of residual geophysical corrections to the measured brightness temperatures that differ significantly from the ascending to the descending side of the orbit. The calibration report [4] explains the separation of the instrument calibration errors from the geophysical corrections, and those derived geophysical errors resemble the signatures seen here. Figure 23 illustrates the residual geophysical brightness temperature errors in ascending and descending data from that analysis. Efforts to understand and correct these errors are the next priority for the science calibration, validation and algorithm working groups. Current evidence indicates that this is primarily an artifact of the model to estimate the galactic reflection diffusion induced by surface roughness. The galaxy progresses across the sky with the seasons, and the core (Milky Way) is brightest in the Southern Hemisphere. The viewing angle of each radiometer beam is different, so each is impacted by the galactic reflection at slightly different points in the sky. Appendix C provides a short analysis of this effect.

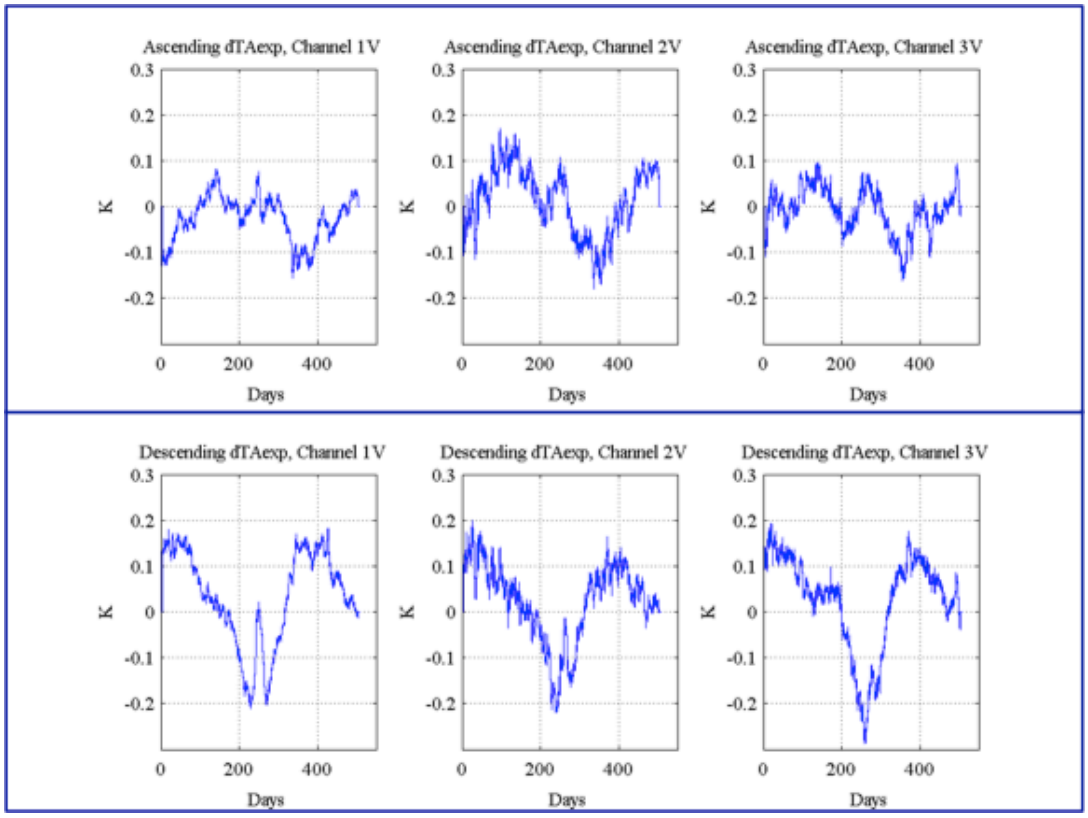

Figure 22. Brightness temperature residuals attributed to geophysical errors after separating the calibration offset [4] for ascending and descending passes. Note similarity with Figure 17.

9. Quantitative error assessments for gridded data

This next discussion compiles results of buoy collocation differences by month, season and latitude bands to quantitatively assess the V2.0 errors relative to the mission accuracy requirements. ESR gridded maps are used, and three monthly maps are averaged for seasonal analyses. As noted above, the buoy matchups are compiled for each 1-degree grid with an average of the buoys within the 150 km radius and with buoy SST>5C. In some tabulations we also compute the expected value of the buoy standard deviations for the grid point matchups.

Figure 24 shows the seasonal-average buoy difference compilations, again demonstrating the annual variation of the salinity errors. Figure 25 provides latitude distributions for the four seasons of Aquarius-buoy bias and standard deviations. The seasonal bias variation is accentuated in high latitudes and noted earlier. The standard deviations hover near 0.2 psu for some seasons and latitudes. Table 2 lists all the numerical values for season and latitude band, and highlights those where the bias and standard deviation are at or less then 0.2, comprising about 25% of the cases.

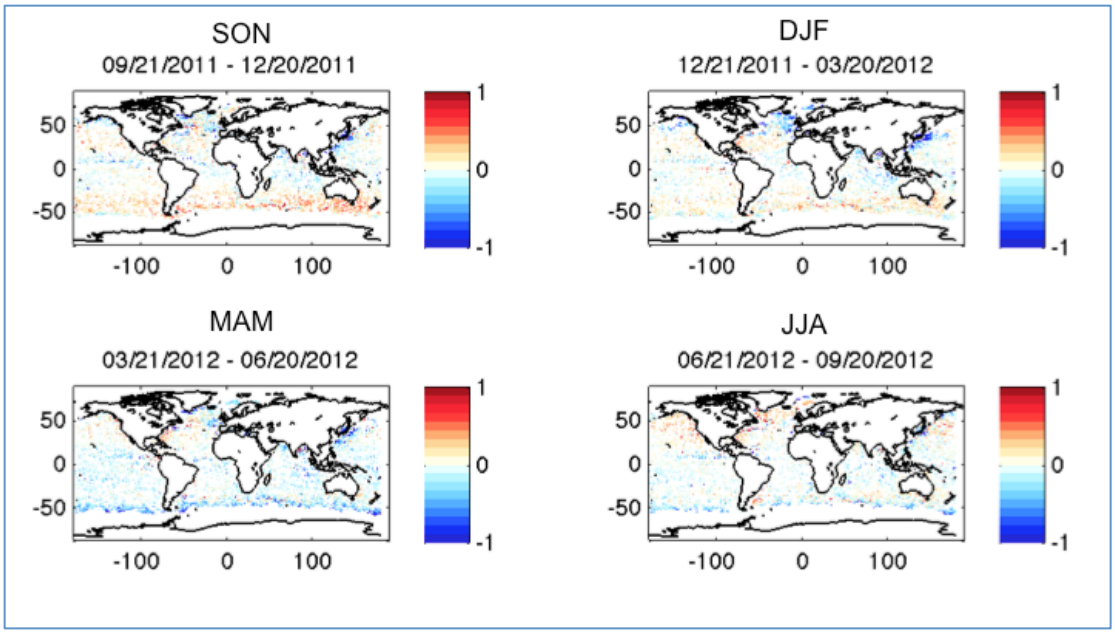

Figure 23. V2.0 Aquarius seasonal buoy difference maps

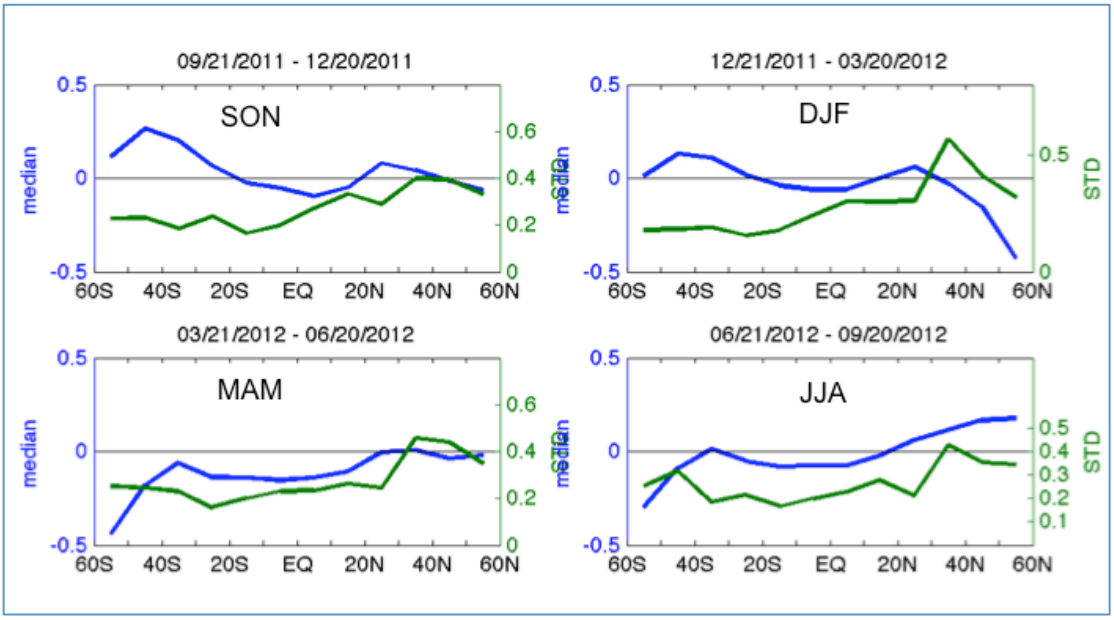

Figure 24. Seasonal average buoy differences by latitude range.

Latitude	SON Bias	SON STD	DJF Bias	DJF STD	MAM Bias	MAM STD	JJA Bias	JJA STD
50-60N	-0.06	0.33	-0.43	0.32	-0.02	0.35	0.18	0.35
40-50N	-0.01	0.39	-0.15	0.41	-0.04	0.44	0.17	0.35
30-40N	0.04	0.40	-0.03	0.57	0.01	0.46	0.11	0.43
20-30N	0.08	0.29	0.06	0.30	0.00	0.24	0.06	0.21
10-20N	-0.05	0.33	0.00	0.30	-0.11	0.26	-0.02	0.28
0-10N	-0.09	0.27	-0.06	0.30	-0.14	0.24	-0.08	0.23
10S-0	-0.05	0.20	-0.06	0.24	-0.15	0.23	-0.07	0.20
10-20S	-0.02	0.16	-0.04	0.18	-0.14	0.20	-0.08	0.17
20-30S	0.06	0.24	0.02	0.16	-0.14	0.16	-0.05	0.22
30-40S	0.20	0.18	0.11	0.19	-0.06	0.23	0.01	0.19
40-50S	0.26	0.24	0.13	0.18	-0.18	0.24	-0.09	0.32
50-60S	0.11	0.23	0.01	0.18	-0.44	0.25	-0.30	0.25

Table 2. Co-located buoy differences for Aquarius V2.0 seasonal average gridded maps, by latitude zones.. Highlighted values have bias and standard deviation within 0.2 psu.

In Table 3, the latitude bands are consolidated between hemispheres, and we also give the estimated buoy standard deviations within those latitude bands. From these we estimate the Aquarius standard deviations as the square-root of the difference between the Aquarius-buoy variance and the buoy variance.

$$\text{Aquarius\_error} = \text{sqrt}(\text{Aquarus-buoy\_STD}^2 - \text{buoy\_STD}^2) \quad (1)$$

These are shown in Table 4, which shows them in reference to the error budget analysis for the mission accuracy requirements. This shows an error allocation by latitude that provides the 0.2 psu global RMS error. Our seasonal mean global RMS estimates are currently about 0.27.

Latitude	SON			DJF			MAM			JJA		
	BIAS	STD	STDb	BIAS	STD	STDb	BIAS	STD	STDb	BIAS	STD	STDb
0-10	-0.07	0.24	0.04	-0.06	0.27	0.03	-0.15	0.23	0.03	-0.07	0.21	0.06
11-20	-0.04	0.26	0.05	-0.02	0.25	0.06	-0.12	0.23	0.06	-0.05	0.23	0.07
21-30	0.07	0.26	0.06	0.04	0.24	0.07	-0.08	0.21	0.06	-0.01	0.22	0.07
31-40	0.15	0.30	0.08	0.08	0.40	0.07	-0.04	0.33	0.07	0.04	0.30	0.08
41-50	0.22	0.31	0.12	0.10	0.29	0.12	-0.16	0.30	0.11	-0.04	0.34	0.10
51-60	0.04	0.30	0.15	-0.04	0.28	0.15	-0.34	0.35	0.14	-0.14	0.39	0.12

Table 3: Seasonal average buoy difference statistics for V2.0 gridded data in consolidated latitude bands (Bias and STD), and buoy standard deviations (STDb).

Minimum Mission Seasonal Salinity Error (psu)		SON	DJF	MAM	JJA
Latitude Range	Allocation (psu)	STDa	STDa	STDa	STDa
0-10	0.15	0.24	0.27	0.24	0.24
11-20	0.16	0.26	0.24	0.26	0.26
21-30	0.16	0.25	0.23	0.25	0.25
31-40	0.18	0.29	0.39	0.29	0.29
41-50	0.21	0.29	0.26	0.29	0.29
51-60	0.24	0.26	0.24	0.26	0.26
61-70	0.26				
Global RMS	0.20	0.26	0.28	0.27	0.27

Table 4. Seasonal standard deviation (STDa) error estimates compared with Minimum Mission Requirements

An alternate analysis is provided in Table 5. Here we use the triple point analyses, as above in Section 4, to estimate the global RMS error for thirteen months and four seasons. The average Aquarius RMSE for the seasonal and monthly Level 3 gridded data are ~0.27 and ~0.3 psu respectively, which are considerably less than the Level 2 point measurements ~0.47 psu presented above. The accompanying estimates for the HYCOM and buoy RMSE are essentially unchanged between the point comparisons and the gridded data analyses.

Yr-Month	Aquarius RMSE	HYCOM RMSE	Buoy RMSE
11-Dec	0.34	0.17	0.16
12-Jan	0.34	0.18	0.13
12-Feb	0.34	0.15	0.16
12-Mar	0.30	0.17	0.15
12-Apr	0.30	0.18	0.16
12-May	0.28	0.19	0.15
12-Jun	0.31	0.17	0.16
12-Jul	0.27	0.19	0.15
12-Aug	0.28	0.18	0.20
12-Sep	0.25	0.19	0.18
12-Oct	0.28	0.19	0.16
12-Nov	0.28	0.19	0.18
12-Dec	0.30	0.19	0.14

2011-12 Season	Aquarius RMSE	HYCOM RMSE	Buoy RMSE
SON	0.26	0.19	0.17
DJF	0.27	0.16	0.14
MAM	0.32	0.17	0.16
JJA	0.26	0.19	0.17

Table 5. Triple point analysis for monthly (left) and seasonal (right) global RMS errors for Aquarius V2.0 data.

Two other preliminary assessments indicate that the 0.2 psu measurement accuracy goal is within reach, at least in certain areas. The first is a comparison with data from the month-long SPURS (Salinity Processes in the Upper Ocean Regional Study) cruise in the central North Atlantic from September to October 2012. *In situ* data were obtained from a variety of near-surface sensors within about a 200x200 km region in the center of the North Atlantic salinity maximum. The *in situ* salinity data are compared with co-located V2.0 Aquarius data in Figure 26, with the RMSD=0.22 (contributed by Y. Chao).

The 28-day (about monthly) average of Aquarius JPL CAP algorithm products [8] derived from the V2.0 data show the RMSD with HYCOM in the range of 0.2 to 0.25 between +/- 40 degrees latitude.

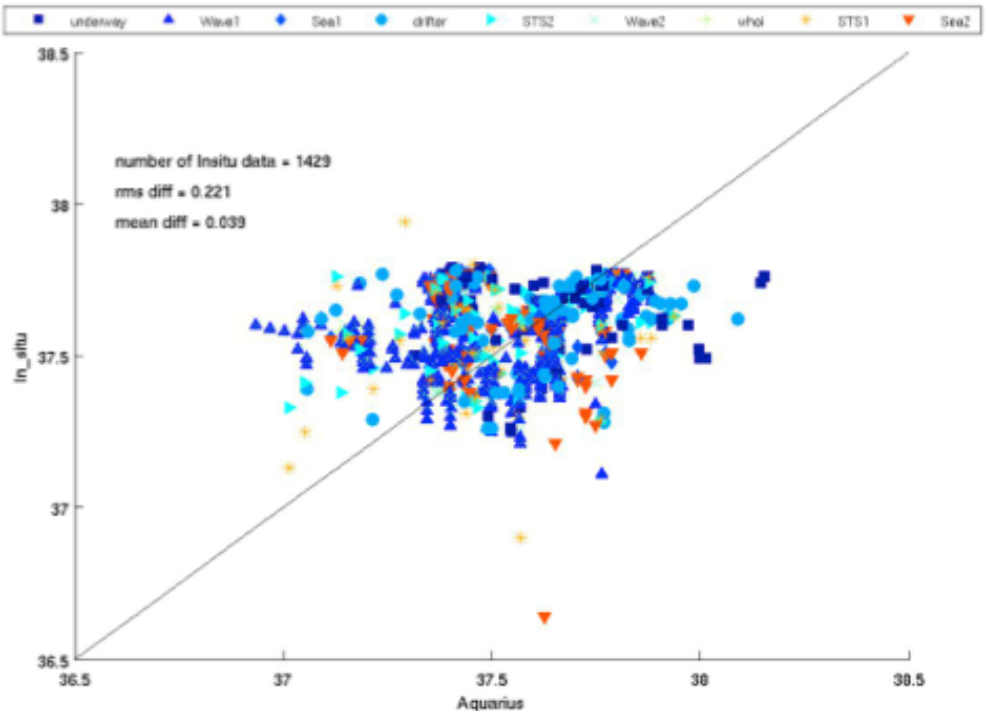

Figure 25. Co-located Aquarius V2.0 and in situ data during the 1-month SPURS cruise in the central subtropical North Atlantic. RMS difference is 0.22 psu. Data processing by Yi Chao

The last example involves the Testbed version of the Level 2 processing code for the next version beyond V2.0. Comparisons of Testbed with TAO/Pirata/RAMA tropical buoy data sampled at ~1m depth give an Aquarius vs buoy RMS error of 0.35 psu for single events and 0.23 psu averaged over 1-month and 150-km. Triple point analysis using Aquarius, HYCOM, and the moored buoys gives an Aquarius RMS error less than 0.2 for the Testbed algorithm for averages over 1-month and 150-km. (contributed by K. Hilburn, T. Meissner and F.Wentz). One should keep in mind that the PMEL buoys are in the warm waters of tropics where the salinity retrieval is most accurate, and that the galactic reflection discussed in Sections 7 and 8 occurs well south of the tropical buoy array. These are preliminary findings and require additional validation. Nevertheless, the results show a steady improvement of the Aquarius retrieved SSS.

10. Mission Science Requirements & compliance matrix.

The Aquarius mission science requirements matrix is shown in Table 6. The two right-hand columns indicate the Baseline and Minimum mission. The fundamental science requirement is to achieve global RMS random errors and systematic biases

no larger than 0.2 psu on 150 km by 150 km scales over the open ocean. The baseline mission requires this on a monthly average, and the minimum mission requires on a seasonal (3-month) average. The triple point analyses presented in Section 9 above indicate that V2.0 global RMS error is ~0.30 monthly and ~0.27 seasonally. The comparable triple point analyses are not shown for V1.3 data because of the geo-location error of the interpolated HYCOM data noted in Section 4. Instead, we estimate V1.3 Aquarius monthly and seasonal RMSE from the V1.3 Aquarius-buoy RMSD using RMSE/RMSD ratios from the V2.0 analysis. These yield V1.3 estimated errors of ~0.44 monthly and ~0.38 seasonally.

	Level 1 Science Mission Requirement	Baseline Mission	Minimum Mission
1	The Aquarius Mission shall collect the space-based measurements to retrieve Sea Surface Salinity (SSS) with global root-mean-square (rms) random errors and systematic biases no larger than **0.2 psu** on 150 km by 150 km scales over the open ocean.	V1.3: 0.44 V2.0 0.30	V1.3: 0.38 V2.0 0.27
2	SSS Averaging Interval	1 Month	3 Months
3	Mission Duration	At least 3 Years	At least 1 Year
4	Deliver data products to a NASA Distributed Active Archive Center (DAAC). Level 1a Reconstructed Unprocessed Instrument Data Level 1b Calibrated Sensor Units Level 2 Derived Geolocated SSS Level 3 Time-space averaged SSS on a standard Earth Projection		Yes

Table 6. Aquarius Mission Science Requirements compliance matrix. The Minimum Mission duration and data product delivery requirements are met. The rms error requirement of 0.2 psu is close but not yet fully achieved with V2.0.

11. Summary, Conclusions and Cautions

This analysis documents the improvements in the V2.0 science data processing and their effect on the Aquarius salinity data. By various measures, the RMS errors are reduced significantly relative to V1.3. With V2.0, we find that the global RMS error is ~0.30 psu monthly and ~0.27 psu seasonally for data that are gridded and smoothed with a 150 km scale.

A key improvement is with the radiometer calibrations, which have essentially removed the quasi-monthly variations from the global comparisons between Aquarius and surface buoy data (see Figure 8). We believe that the sensor

calibrations are well resolved. The residual errors in the data are attributed to errors in the geophysical corrections to the measured brightness temperatures.

In particular, there is still a residual salinity error with a yearly cycle. This is most likely related to residual errors in the correction for galactic reflection and perhaps other terms of some celestial origin. This annual cycle is manifest most clearly in contrasting the ascending and descending sides of the orbit, and is dominantly in the Southern Hemisphere and in the descending phase of the orbit. This yearly error cycle remains apparent when the full orbit is used to generate gridded maps because of the asymmetry of the error between the ascending and descending phases. These processes are a high priority to be remedied in the next data release.

Note of Caution, Annual Cycle: It is strongly recommended that data users refrain from analyzing or drawing conclusions about the annual salinity cycle in the V2.0 data, because the variability is dominated by these spurious, non-oceanographic, error signals, especially in the Southern Hemisphere and higher latitudes.

Localized persistent biases between ascending and descending passes appear to be linked to radio frequency interference (RFI) that is not completely corrected by the RFI filter. The RFI will bias the brightness temperatures toward the positive, thus the salinity will be biased negative. These regions are primarily in the eastern N. Atlantic adjacent to Europe where it is likely that the ascending pass is contaminated as the antenna faces the European subcontinent. Likewise, the western N. Atlantic and Asia-Pacific regions are biased on the descending pass when the antenna views westward. We do not yet have an effective flag for these situations, and the standard gridded Level 3 data presently do not exclude them. However, there will be separate gridded ascending and descending L3 fields, and users can difference these to evaluate whether these persistent features may be a problem in their regions of interest.

Note of Caution, RFI: Persistent negative salinity bias my be present in some regions due to RFI. Users should be very cautious with using ascending pass data in the eastern N. Atlantic and descending pass data in the western N. Atlantic and Asia-Pacific regions.

One other important feature appearing in the ascending-descending difference maps is the residual zonal band across the tropical Pacific, especially during the boreal autumn. This partly aligns geographically with the Pacific ITCZ and associated low salinity zone. As noted above, this is zone is aligned with the magnetic equator and the problem most likely is related to cross-polarization coupling in the antenna pattern correction. This has been corrected in V2.0, but evidently some additional tuning may be needed.

Note of Caution, Pacific ITCZ: A zonal pattern of salinity difference between ascending and descending passes is partly aligned with the Pacific ITCZ. This is mostly evident in the fall. Users should use caution when analyzing data from this region.

12. References

1. Lagerloef, et al, Oceanograhy, 2008
2. Le Vine, D.M., G.S.E. Lagerloef, F.R. Colomb, S.H. Yueh, and F.A. Pellerano. 2007. Aquarius: An instrument to monitor sea surface salinity from Space IEEE Transactions on Geoscience and Remote Sensing 45 (7):2,040–2,050.
3. Aquarius V2.0 Algorithm Theoretical Basis Document (ATBD) [AQ-014-PS-0017]
4. Aquarius Radiometer Post-Launch Calibration for Product Version 2 [AQ-014-PS-0015]
5. Reynolds, R. W., T. M. Smith, C. Liu, D. B. Chelton, K. S. Casey, and M. G. Schlax, 2007: Daily high-resolution blended analyses for sea surface temperature. J. Climate, 20, 5473-5496.
6. Chassignet, E.P., H.E. Hurlburt, E.J. Metzger, O.M. Smedstad, J. Cummings, G.R. Halliwell, R. Bleck, R. Baraille, A.J. Wallcraft, C. Lozano, H.L. Tolman, A. Srinivasan, S. Hankin, P. Cornillon, R. Weisberg, A. Barth, R. He, F. Werner, and J. Wilkin, 2009. U.S. GODAE: Global Ocean Prediction with the HYbrid Coordinate Ocean Model (HYCOM). Oceanography, 22(2), 64-75.
7. Yueh, S and J Chaubell, "Sea Surface Salinity and Wind Retrieval using Combined Passive and Active L-Band Microwave Observations", IEEE Trans. Geosci. Remote Sens., Vol. 50, No. 4, pp. 1022-1032, April 2012.
8. Yueh, S. W. Tang, A. Fore, G. Neumann, A. Hayashi, A. Freedman, J. Chaubell, and G. Lagerloef, "L-band Passive and Active Microwave Geophysical Model Functions of Ocean Surface Winds and Applications to Aquarius Retrieval," submitted to IEEE TGRS, July 2012.
9. E.J. Metzger, O.M. Smedstad, P. Thoppil, H.E. Hurlburt, A.J. Wallcraft, D.S. Franklin, J.F. Shriver, and L.F. Smedstad, 2008: Validation Test Report for the Global Ocean Prediction System V3.0 – 1/12° HYCOM/NCODA: Phase I. NRL Memo. Report, NRL/MR/7320--08-9148.
10. E.J. Metzger, O.M. Smedstad, P.G. Thoppil, H.E. Hurlburt, D.S. Franklin, G. Peggion, J.F. Shriver, T.L. Townsend, and A.J. Wallcraft, 2008: Validation Test Report for the Global Ocean Prediction System V3.0 – 1/12° HYCOM/NCODA: Phase II. NRL/MR/7320--10-9236.

Appendix A: The NAVO/FSU HYCOM data are obtained from the global 1/12° data-assimilative HYCOM model along with the Navy Coupled Ocean Data Assimilation (NCODA) system at the Naval Oceanographic Office (NAVOCEANO). The HYCOM data are available from the HYCOPM data server http://tds.hycom.org/thredds/GLBa0.08/expt_90.9.html?dataset=GLBa0.08/expt_90.9.

This HYCOM run assimilates available along track satellite altimeter observations, satellite and in situ sea surface temperature as well as in situ vertical temperature and salinity profiles from XBTs, ARGO floats, and moored buoys. In terms of near surface salinity forcing, HYCOM uses monthly climatology of river discharges (applied at the top 6 meters of the model) and relaxation to monthly SSS climatology (at 15 m) with a restoring time scale of 30 days, in addition to E-P forcing. Both the climatological river forcing and near surface salinity relaxation are intended to prevent the HYCOM simulation from drifting away from climatology, but at the same time they may suppress non-seasonal variations occurring in nature. The NCODA system is based on a multi-variate Optimal Interpolation (MVOI) scheme. Because of the assimilation of Argo floats and buoy data, the HYCOM analysis is not independent of Argo and buoys. Moreover, the nature of the assimilation could also introduce some level of correlation between the errors of the HYCOM analysis field and the errors of Argo and buoy SSS. More details of this HYCOM solution can be found in [6], [9] and [10].

Appendix B: Triple point uncertainty estimate of Aquarius and validation data

The satellite salinity measurement S_S and the *in situ* validation measurement S_V are defined by:

$$S_S = S \pm \varepsilon_S$$

$$S_V = S \pm \varepsilon_V$$

where S is the true surface salinity averaged over the Aquarius footprint area and microwave optical depth in sea water (~ 1 cm). ε_S and ε_V are the respective satellite and *in situ* measurement errors relative to S. The mean square of the difference ΔS between S_S and S_V is given by:

$$\langle \Delta S_{SV}^2 \rangle = \langle \varepsilon_S^2 \rangle + \langle \varepsilon_V^2 \rangle \quad (1)$$

where $\langle\ \rangle$ denotes the average over a given set of paired satellite and *in situ* measurements, and $\langle \varepsilon_S \varepsilon_V \rangle = 0$.

Likewise, define HyCOM salinity interpolated to the satellite footprint as $S_H = S \pm \varepsilon_H$, and mean square differences

$$\langle \Delta S_{HV}^2 \rangle = \langle \varepsilon_H^2 \rangle + \langle \varepsilon_V^2 \rangle \quad (2)$$ HyCOM vs in situ validation data

$$\langle \Delta S_{SH}^2 \rangle = \langle \varepsilon_S^2 \rangle + \langle \varepsilon_H^2 \rangle \quad (3)$$ Satellite vs HyCOM

Equations (1)-(3) comprise three equations with three variables given by:

$$\langle \varepsilon_S^2 \rangle = \{ \langle \Delta S_{SV}^2 \rangle + \langle \Delta S_{SH}^2 \rangle - \langle \Delta S_{HV}^2 \rangle \} /2 \quad (4)$$ satellite measurement error

$$\langle \varepsilon_H^2 \rangle = \{ \langle \Delta S_{SH}^2 \rangle + \langle \Delta S_{HV}^2 \rangle - \langle \Delta S_{SV}^2 \rangle \} /2 \quad (5)$$ HyCOM measurement error

$$\langle \varepsilon_V^2 \rangle = \{ \langle \Delta S_{SV}^2 \rangle + \langle \Delta S_{HV}^2 \rangle - \langle \Delta S_{SH}^2 \rangle \} /2 \quad (6)$$ In situ validation measurement error

Appendix C: TA model errors; ascending, descending and reflected galaxy (contributed by Liang Hong)

TA is defined as the measured brightness temperature at the antenna, after the RFI filter, and TA_{exp} is the modeled (or expected value). The difference between these, $dTA = Tf - TA_{exp}$, contains a combination of errors in both instrument calibration and geophysical model. These errors in each channel present long term temporal variations as seen in first and last column of plots in Figure C1, where estimated calibration errors have been removed. Assuming instrument does not have orbital variation, and long term drifts are negligible within an orbit, residual calibration error is a common part in both ascending and descending paths. The difference between the two should be differences in geophysical model errors that are not cancelled out. From the middle columns of the plots in Figure C1, it is obvious that geophysical model errors behave differently in ascending and descending passes.

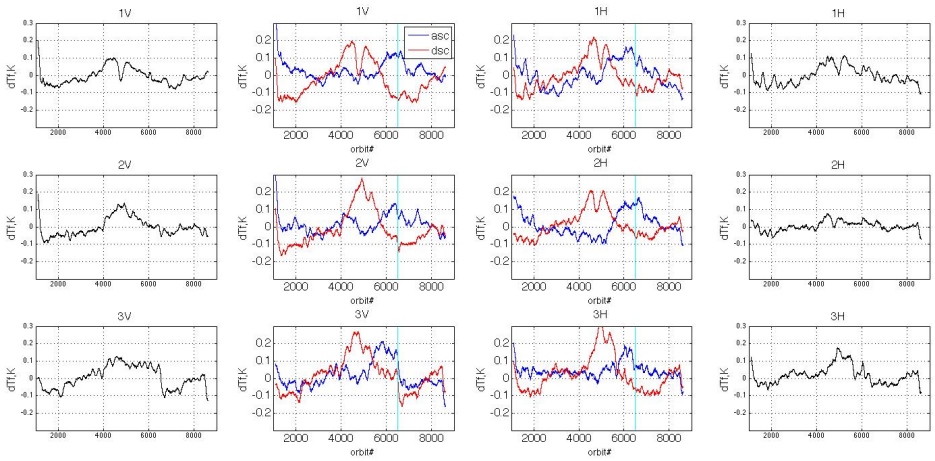

Figure C1. dTA of each orbit and of separated Asc/Dsc paths

By comparing the annual pattern of the difference of dTA's between ascending and descending paths (ddTf) with all geophysical inputs, it is observed that the galactic effects have very similar annual variation, as shown in Figure C2. The green curve in each plot is a simple linear regression of these weighted difference of direct and reflected galactic correction to fit ddTf. The very good match of green curves to blue curves implies possible corrections for galactic effects applied in the TA_{exp} calculation.

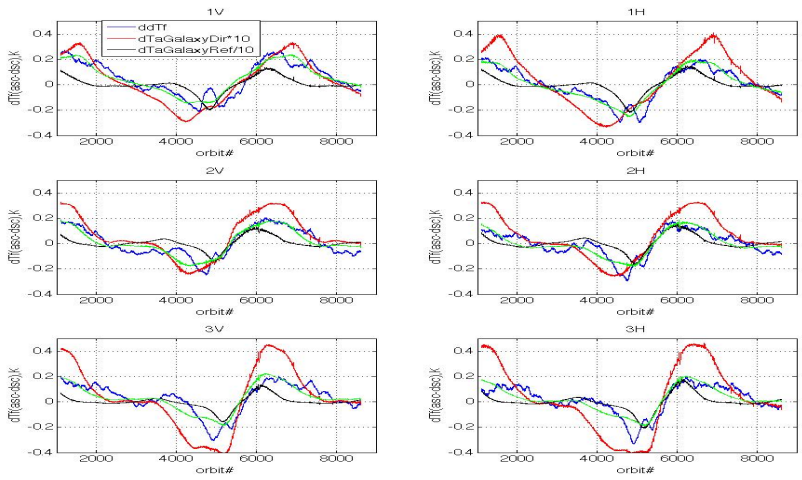

Figure 26. Galactic effects in Asc/Dsc; ddTf = dTA_Asc – dTA_Dsc, dTa_GalaxyDir is Asc/Dsc difference of correction for direct galactic brightness, dTa_GalaxyRef is Asc/Dsc difference of correction for reflected galactic brightness.

Following the idea, linear regressions are done to adjust the galactic brightness's in modeled TA_{exp}. With footprints in ascending and descending paths separated, coefficients are computed in the following equation,

$$dTA_{new} = dTA + c0 + c1 * Ta\_Galaxy\_dir + c2 * Ta\_Galaxy\_ref$$

After adjustment to galactic brightness's is applied, the annual variation in each channel is greatly reduced as seen in both the dTA (combined ascending and descending paths) and the difference between dTA's of ascending and descending paths, as seen in Figure C3.

These calculations are preliminary, and results are not applied to V2.0 data.

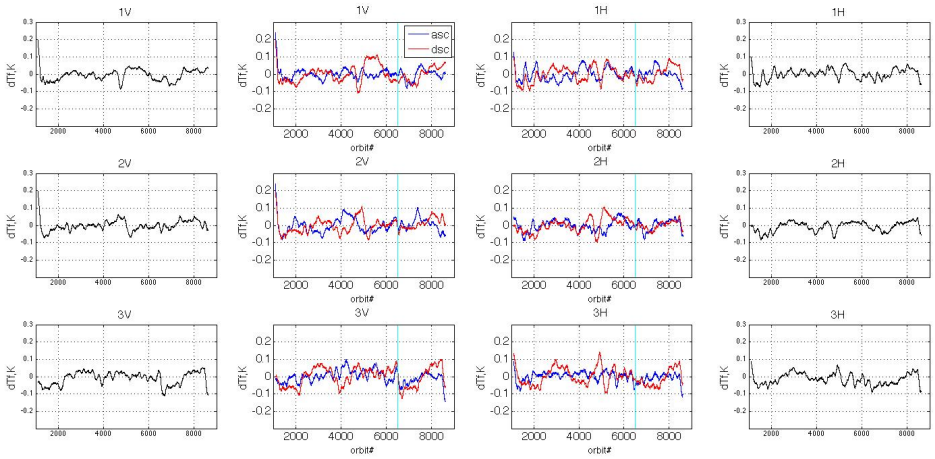

Figure C3. dTA with galactic Correction

End of document